Graduate School of Oceanography Faculty Publications

Graduate School of Oceanography

2001

Absolute geostrophic velocity within the Subantarctic Front in the Pacific Ocean

Kathleen A. Donohue
University of Rhode Island, kdonohue@uri.edu

Erin Firing

Shuiming Chen

Follow this and additional works at: https://digitalcommons.uri.edu/gsofacpubs

Absolute geostrophic velocity within the Subantarctic Front in the Pacific Ocean

Absolute geostrophic velocity within the Subantarctic Front in the Pacific Ocean

Kathleen A. Donohue

Graduate School of Oceanography, University of Rhode Island, Narragansett

Eric Firing and Shuiming Chen

Department of Oceanography, University of Hawaii, Honolulu

Abstract. Velocity measurements from a shipboard acoustic Doppler current profiler (ADCP) are used as a reference for geostrophic current calculations on six sections across the Subantarctic Front (SAF) in the Pacific Ocean. The resulting cross-track velocity estimates near the bottom range from 4 to 10 cm s^{-1} to the east in the eastward jet at the SAF; in adjacent regions of westward surface flow, the near-bottom velocity is usually to the west. On one section where simultaneous lowered ADCP velocity profiles are available, they confirm the results from the shipboard ADCP. Annual mean velocity sections from the Parallel Ocean Program numerical model also show near-bottom velocities exceeding 5 cm s^{-1}, with the same tendency for the zonal velocity component near the bottom to match the direction of the surface jets. Transport across the entire Antarctic Circumpolar Current (ACC) cannot be estimated accurately from ADCP-referenced geostrophic sections because even a very small cross-track bias integrates to a large error. A preliminary look at the 1992 model transport stream function shows that the effect of bottom-referencing varies from section to section; it can cause 40-Sv recirculations to be missed, and can cause net transport to be underestimated or overestimated by $O(30 \text{ Sv})$.

1. Introduction

The Antarctic Circumpolar Current (ACC) is characterized by a series of property gradient fronts coincident with geostrophic jets. Though narrow, often less than 50 km wide, the frontal jets encompass about 75% of the eastward ACC transport [*Nowlin and Clifford*, 1982; *Whitworth and Nowlin*, 1987; *Read et al.*, 1995]. The transport of the ACC through Drake Passage was carefully estimated during the International Southern Ocean Studies (ISOS) program using an extensive array of closely spaced deep current meter moorings to reference geostrophic velocity calculations from shipboard hydrographic sections *Whitworth et al.* [1982]. Elsewhere, velocity observations are sparse, so geostrophic shears are generally referenced to zero at the bottom [e.g., *Whitworth and Nowlin*, 1987]. Two questions arise. Does the bottom reference distort the horizontal velocity structure? If so, does it bias estimates of the ACC transport?

Results from the Fine Resolution Antarctic Model (FRAM) suggest a positive answer to each of these ques-

tions. The model shows a tendency for the velocity to behave in an equivalent-barotropic mode; near-bottom velocities are reduced in magnitude but remain in the same direction relative to the surface velocities [*Killworth*, 1992]. Instantaneous snapshots of the velocity field show that eastward velocity within the ACC jets extends throughout the water column [*Webb et al.*, 1991]; in FRAM, a bottom reference would bias the transport low. FRAM transport through Drake Passage is about 50 Sv larger than observations, however [*Grose et al.*, 1995], casting doubt on the accuracy FRAM's currents elsewhere as well. Now that global general circulation models with substantially finer resolution than FRAM are available, it is time to revisit the questions of ACC structure and transport in numerical models. In this paper we will look briefly at one such model, the Parallel Ocean Program (POP) high-resolution global ocean model [*Maltrud et al.*, 1998].

Recent observations from the World Ocean Circulation Experiment Hydrographic Program (WHP) provide another opportunity to address these questions, however, and that is the primary topic of this work. Specifically, we use shipboard acoustic Doppler current profiler (SADCP) observations to reference geostrophic current sections from WHP cruises. Because they are simultaneous with hydrographic measurements and because they can be integrated between stations, SADCP

Table 1. World Ocean Circulation Experiment Hydrographic Program Lines in the Pacific Sector of the Southern Ocean

Line	Date	Longitude	Ship
P14	Jan. 1996	175°E	*Discoverer*
P15	Jan.-Feb. 1996	170°W	*Discoverer*
P16	Oct. 1992	150°W	*Knorr*
P17	Oct.-Nov. 1992	135°W	*Knorr*
P17	Dec. 1992	126°W	*Knorr*
P18	Feb. 1994	103°W	*Discoverer*
P19	Jan. 1993	88°W	*Knorr*

currents are a logical and common choice as a geostrophic reference [e.g., *Pickart and Lindstrom*, 1994; *Saunders and King*, 1995; *Cokelet et al.*, 1996]. In many instances, the SADCP has shown the absence of a level of no motion; *Saunders and King* [1995] found strong barotropic flow in the Falkland Current system, *Meinen et al.* [2000] cited enhanced transports within the North Atlantic Current and barotropic recirculations inshore of the North Atlantic Current, and *Heywood et al.* [1999] showed that the southernmost ACC jet has eastward top-to-bottom velocities. All of these features would be missed by referencing geostrophic shears to the bottom.

Here we show geostrophic velocities referenced to the SADCP along six WHP lines that crossed the ACC in the Pacific Ocean. Along parts of the lines, bad weather caused ADCP data dropouts and/or strong ageostrophic motion, rendering the SADCP data unusable as a geostrophic reference. By chance, however, conditions were always adequate for SADCP referenc-

ing in the vicinity of the Subantarctic Front (SAF), the northernmost jet in the ACC; therefore we concentrate on the SAF. There, the SADCP-referenced geostrophic velocities show that a bottom reference underestimates the eastward flow associated with the SAF, and also underestimates the westward flow in the westward limbs of adjacent recirculations or eddies. Along the one section where lowered acoustic Doppler current profiles (LADCP) sampled the SAF, they confirm the SADCP result. We also show a longer ADCP-referenced current section from the one WHP line with the best SADCP data coverage, P19 (88°W), which confirms the tendency for ACC geostrophic bottom velocities to be in roughly the same direction as the geostrophic surface velocities.

2. Data

Seven WHP lines in the Pacific sector of the Southern Ocean were occupied during the period 1992–1996 (Table 1). Station spacing for the full-depth hydrographic profiles was typically 55 km, with closer spacing near topographic features and ACC fronts [*McTaggart et al.*, 1996; *McTaggart and Johnson*, 1997; *Rubin et al.*, 1998; *Daly et al.*, 2001]. SADCP measurements were made on all lines, but were not sufficiently accurate for present purposes on one of them, P18. Three of the lines include LADCP profiles, but only on P15 did they sample the SAF. That leaves six sections with hydrographic and velocity measurements in the SAF (Plate 1).

The LADCP measurements on P15 were made with a 153-kHz broadband sonar from RD Instruments (RDI).
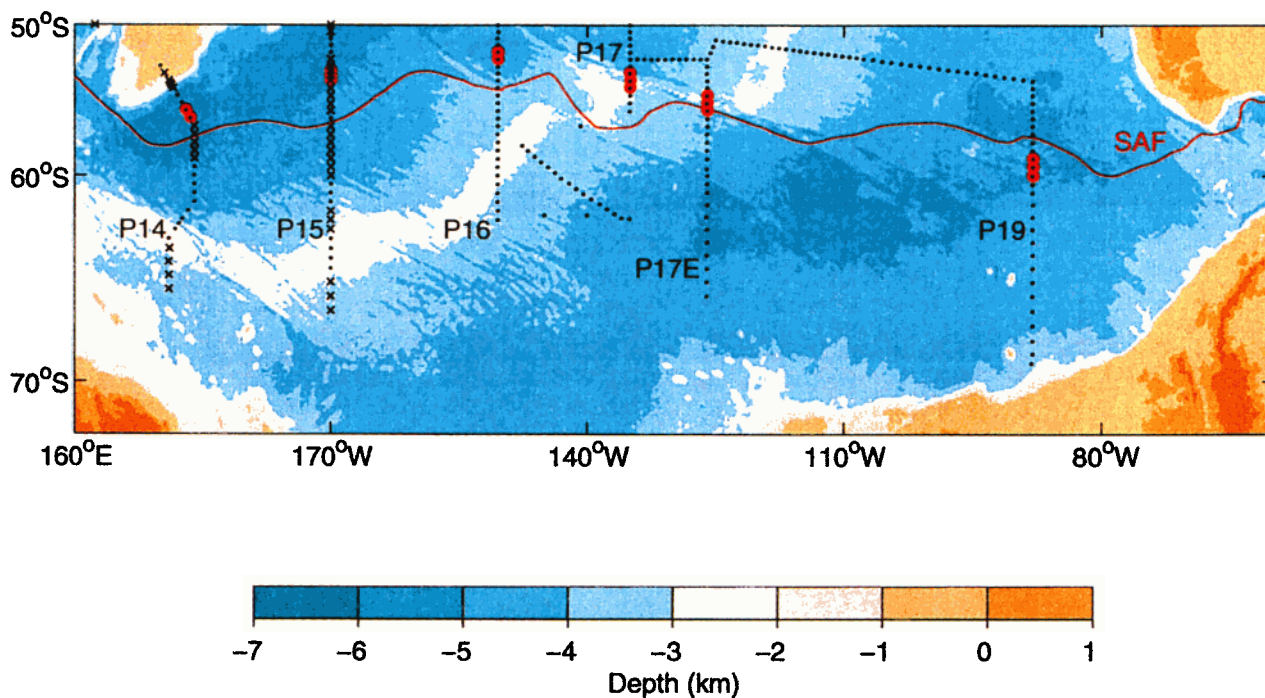
Plate 1. Positions of hydrographic stations are shown as black dots. Solid continuous red lines show the positions of the Subantarctic Front (SAF) determined from historical hydrographic data by *Orsi et al.* [1995]. Using their criteria, we identify the SAF along the World Ocean Circulation Experiment Hydrographic Program (WHP) lines (red circles). Shipboard acoustic Doppler current profiler (SADCP) data are available for all lines. Lowered acoustic Doppler current profiler (LADCP) stations are noted by the crosses.

Details of LADCP instrumentation and processing have been given by *Hacker et al.* [1996] and *Fischer and Visbeck* [1993]. Uncertainty in the barotropic component of LADCP profiles is typically about 1 cm s^{-1}, but compass errors owing to the proximity of P15 to the magnetic pole probably increase the barotropic error to 2 cm s^{-1}. The uncertainty in velocity at any given depth is larger and harder to quantify; 2–4 cm s^{-1} is a reasonable estimate. Waters at high latitudes tend to have good deep scattering amplitudes, minimizing the depth-dependent part of the velocity error.

SADCP data were collected using RDI 150-kHz narrowband systems. Real-time processing resulted in 2.5-min (P16 and P17) or 5-min (P14S, P15S, P17E, and P19S) vector averages with 8-m vertical resolution. Compass errors were measured with an Ashtech 3DF GPS attitude sensor [*King and Cooper*, 1993], and velocities were corrected accordingly. Standard water track calibration methods [*Joyce*, 1989; *Pollard and Read*, 1989] provided a velocity scale factor and constant angular offset between the transducer and the Ashtech antenna array. The inherent accuracy of the 3DF together with the consistency of successive calibrations on a given ship indicate that heading accuracy better than 0.1° was achieved, and the corresponding cross-track velocity errors are under 1 cm s^{-1}.

3. SADCP Reference Technique

The geostrophic velocity is referenced to the SADCP by matching the integrated geostrophic shear to the cross-track SADCP velocity. In the horizontal we average between stations; in the vertical we average over the thickest layer for which the SADCP velocities are consistently available, but avoiding the surface layer where near-inertial energy is usually highest. Here, we average from 150 m to 350 m, except in a few cases where the SADCP range did not extend this deep. The bottom velocity is defined as the offset between the geostrophic velocity referenced to the bottom and the geostrophic velocity referenced to the SADCP (Figure 1). Note that the bottom velocity is not the velocity at the base of the water column; rather, it is the geostrophic velocity at the deepest common level.

As noted by *Saunders and King* [1995], a correction must be made when the momentum balance includes inertial terms. In regions of strong curvature, such as eddies, the flow is in gradient-wind balance rather than geostrophic balance. The relationship between geostrophic velocity V_g and the gradient-wind velocity V, written in natural coordinates and solved for V_g from *Holton* [1979] is

$$V_g = V(1 + \kappa \frac{V}{f}), \qquad (1)$$

where κ is curvature defined as positive for flow turning to the left, and f is the Coriolis parameter. In small, intense eddies, the geostrophic shear must be matched not to V measured by the ADCP, but to V_g from (1).
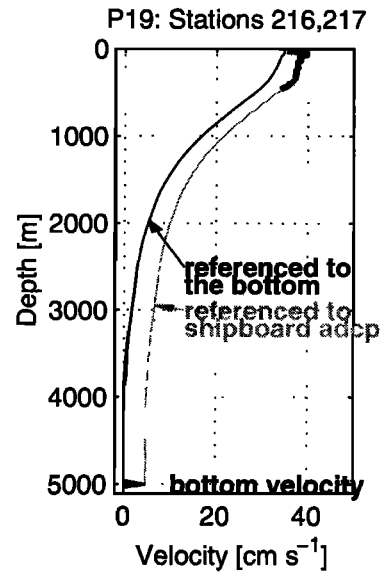

Figure 1. Geostrophic velocity referenced to the bottom (solid) and to the SADCP (shaded) for SAF station pair 216, 217 along P19. The thick solid line is the SADCP cross-track velocity averaged between the stations. The offset between the two velocity estimates is defined as the "bottom velocity".

The center of the eddy is found from the ADCP velocity vectors in a manner similar to *Saunders and King* [1995]. In an axisymmetric eddy, the vectors normal to the velocity vectors will intersect at the center of the eddy (Figure 2).

Errors in the SADCP reference derive mainly from two sources: instrument error and ageostrophic motion. The major contributors to the SADCP-measured ageostrophic motion are assumed to be barotropic tides, internal tides (exclusively semidiurnal poleward of 30°) and near-inertial oscillations. The barotropic tide as estimated using the OSU TOPEX/Poseidon Cross-Over Global Inverse Solution, version 3.1 [*Egbert et al.*, 1994] has been removed from our SADCP and LADCP profiles. The predicted tide is less than 1.5 cm s^{-1} except near Campbell Plateau, where it exceeds 3 cm s^{-1}; the error after removal of the predicted tide is considered negligible. Separately, we estimate that baroclinic tides and near-inertial motions would each yield a reference velocity standard deviation of about 2 cm s^{-1} (Appendix A). Adding their variances to that of an independent instrument error estimated as 1 cm s^{-1} standard deviation, the square root of the sum yields a net reference layer standard deviation of about 3 cm s^{-1} (Table 2).

A comparison between the geostrophic shear and the between-station cross-track SADCP velocity profile gives an independent estimate of the ageostrophic velocity at small vertical scales (Figure 3). (The comparison for all the profiles along P19 is not shown but is similar in character.) The standard deviation of the difference between the SADCP and geostrophic velocity profiles over the reference depth interval ranges from
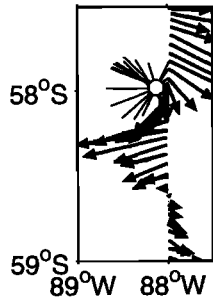
Figure 2. SADCP velocity vectors along P19 (88°W). The center of the eddy (circle) is determined by the intersection of normals to the velocity vectors (thin lines).

0.2 to 1.9 cm s^{-1}, showing that for most profiles, the reference velocity is not sensitive to the choice of depth range.

4. Velocity in the SAF

The SAF locations along the WHP lines are identified using the criteria from *Orsi et al.* [1995] (Plate 1). Briefly stated, the SAF is the poleward boundary of the Subantarctic Mode Water thermostad [*McCartney*, 1977, 1982] and the SAF is also coincident with a rapid northward deepening of the near-surface salinity minimum [*Whitworth and Nowlin*, 1987]. The WHP locations differ from the historical analysis of *Orsi et al.* [1995] by as much as 3°-4° of latitude. We do not know why the discrepancy is so large; the SAF definition is essentially the same. Possible factors include temporal variability and spatial gaps in the historical data.

Before examining the details of the SADCP reference applied to the SAF regions several general features evident in Plates 2 and 3 are highlighted. First, the SAF often coincides with a sea surface temperature front. Second, SADCP velocity vectors distinguish jets associated with the SAF from adjacent eddies. Third, strong bottom velocities (>3 cm s^{-1}) can be found in the eddies. Finally, bottom velocities are eastward within the SAF (Table 3).

4.1. P14 173.3°E

Results for P14, the westernmost line, are shown in Plate 2. North of 57°S, surface velocity vectors are northeast, roughly parallel to the Campbell Plateau bathymetric contours. A cyclonic eddy centered near 55°S interrupts this eastward flow. Geostrophic transport referenced to the bottom is also mainly eastward along P14, concentrated at the SAF station pair, and with westward transport near the eddy. Among the sections we studied, P14 has the largest predicted barotropic tide; the large SADCP reference errors determined from the on-station analysis (3.7 cm s^{-1}) are presumably due to strong internal tides near Campbell Plateau. This is visible in the increased rms of the SADCP-

geostrophic shear fit for station pairs near the plateau (stations 6 through 9 in top panels of Figure 3). The bottom velocities from the SADCP reference indicate that a zero velocity at the bottom will underestimate the eastward flow within the SAF and in the region of eastward flow along the Campbell Plateau. Beneath the SAF the inferred bottom velocity is 10.1±3.7 cm s^{-1}. The SADCP reference also shows strong bottom velocities of about 10 cm s^{-1} associated with the cyclonic eddy north of the SAF. The curvature correction for the cyclone increases the westward bottom velocity estimate at station pair 10-11 from 7.2 cm s^{-1} to 9.7 cm s^{-1}. At station pair 9-10 the correction is less than 1 cm s^{-1}.

4.2. P15 170°W

The most striking features along P15 are two eddies bracketing the SAF, an anticyclone to the north and a cyclone to the south (Plate 2). The velocity vectors show the resulting strong convergence into the SAF. Another anticyclonic eddy is found in the southern portion of P15 near 56.3°S. The bottom reference yields eastward transport for four station pairs surrounding the SAF with peak transport at the SAF. The SADCP reference shows strong eastward bottom velocities near the SAF. The strongest eastward bottom velocity is located at the northern SAF station pair (7.9±2.5 cm s^{-1}). Away from the SAF and eddies, the SADCP reference shows small bottom flow that does not exceed the SADCP reference error. The curvature adjustment has been applied to the three eddies. The adjustment is less than 1 cm s^{-1} except for station pair 59-60, where the curvature adjustment decreases the eastward bottom velocity from 9.8 cm s^{-1} to 7.9 cm s^{-1}, consistent with the fact that gradient-wind velocities in an anticyclone exceed the geostrophic velocities.

Table 2. Contributions to Uncertainty in the Shipboard Acoustic Doppler Current Profiler (SADCP) Referenced Velocity[a]

Line	Instrument	Semidiurnal	Near-Inertial	Total
P14	1.0	2.8	2.2	3.7
P15	1.0	1.2	1.9	2.5
P16	1.0	2.6	2.1	3.5
P17	1.0	2.3	1.6	3.0
P17E	1.0	1.8	1.4	2.5
P19	1.0	1.3	1.8	2.4

[a]Values are in cm s^{-1} (one standard deviation). The total is the root-mean-square of the three contributions.
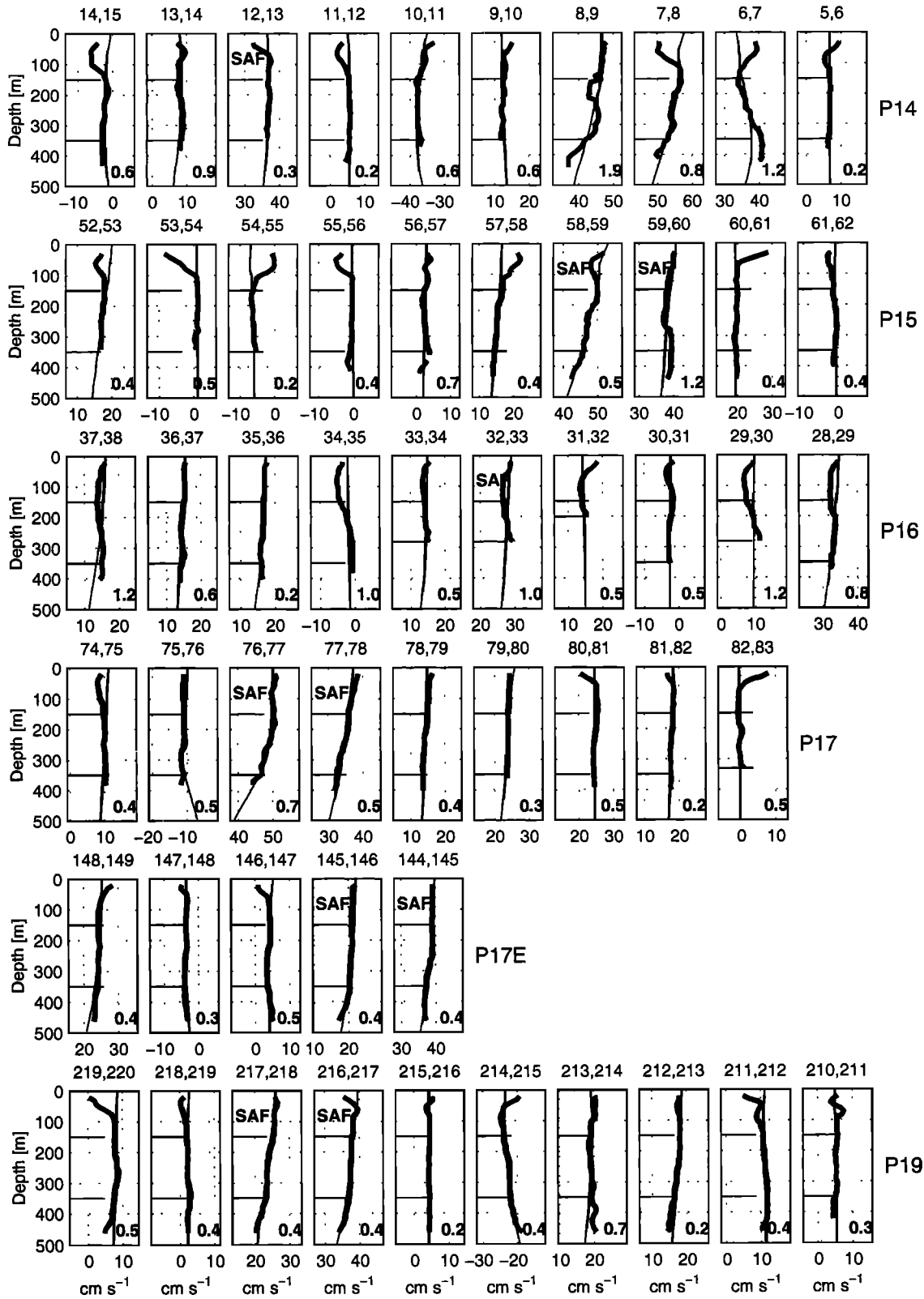
Figure 3. Comparison between the SADCP-referenced geostrophic velocity (thin line) and the average SADCP cross-track velocity (thick line) for stations pairs near the SAF along each WHP line. In the bottom right corner of each plot, the rms of the difference between the two velocities over the reference depth interval ranges (horizontal lines) in cm s^{-1} is shown. The rms values range from 0.2 to 1.9 cm s^{-1}, indicating that the ageostrophic noise is minimal and that the reference velocity is not sensitive to the choice of reference depth range. Numbers above each plot denote station pairs.

Table 3. Velocities Within the Subantarctic Front (SAF)[a]

Line	Latitude	Longitude	U_g cm s^{-1}	U_a cm s^{-1}	Bottom Velocity cm s^{-1}	Deepest Common Level m
P14	56.2°S	173.3°E	26.4	36.5	10.1 ± 3.7[b]	5341
P15	53.8°S	170.0°W	51.4	53.0	1.6 ± 2.5	5128
P15	53.5°S	170.0°W	32.8	40.7	7.9 ± 2.5[b]	5059
P16	52.3°S	150.5°W	20.5	29.1	8.6 ± 3.5[b]	4336
P17	54.2°S	135.0°W	46.1	50.2	4.1 ± 3.0[b]	2707
P17	53.8°S	135.0°W	33.8	37.4	3.6 ± 3.0[b]	2473
P17E	55.3°S	126.0°W	27.9	39.9	11.9 ± 2.5[b]	3378
P17E	55.7°S	126.0°W	22.8	22.3	-0.5 ± 2.5	3378
P19	59.2°S	88.0°W	34.8	39.6	4.8 ± 2.4[b]	4990
P19	59.8°S	88.0°W	19.4	26.1	6.7 ± 2.4[b]	4990

[a]U_g (U_a) are the surface geostrophic velocities referenced to the bottom (SADCP). The bottom velocity is U_a - U_g. The deepest common level is given in meters.

[b]SADCP bottom velocities exceed zero by more than one standard deviation.

Contours of LADCP velocity for the SAF region along P15 support the conclusion from the SADCP reference: Zonal velocities associated with the SAF extend throughout the water column (Figure 4). Similar to the SADCP reference, the strongest near-bottom velocities are shifted to the north relative to the near-surface maximum. Below about 2000 m the zonal velocity within the SAF is nearly uniform with depth, and maximum speeds are about 12 cm s^{-1} (station 59, 53.67°S). The meridional velocities also show the deep penetration of the surface flows; the convergence into the SAF extends throughout the water column. The qualitative comparison between the directly measured deep flows and the inferred deep flows from the SADCP reference is good, and it is tempting to try to quantify the agreement by comparing transports. This is not done here for two reasons. The mean and standard deviation of the difference between the on-station SADCP and LADCP velocities averaged over the same depth range for stations 54 to 62 (56°E to 52.5°E) are -2.1 ±2.0 cm s^{-1} for the zonal component and -0.2 ±1.9 cm s^{-1} for the meridional component. This suggests an eastward bias in the LADCP velocities, probably due to compass error (J. Hummon and E. Firing, unpublished manuscript, 1999). A 2-cm s^{-1} bias leads to a 40-Sv error in transport over 3.5° for a 5000-m water depth. Additionally, the LADCP does not integrate between stations, so errors in transport occur when the sampling does not fully resolve the flow. The station spacing on this line is indeed too wide for good transport estimates: When only on-station data are used, the SADCP underestimates upper ocean eastward transport for this section by about 15%. Therefore the LADCP estimate of eastward transport would be overestimated owing to instrument bias and underestimated owing to inadequate horizontal sampling.

4.3. P16 150.5°E

The geostrophic transports referenced to the bottom are eastward for all station pairs along P16 (Plate 2).

Bottom velocities are zero or slightly westward away from the SAF but strongly eastward within the SAF, with speeds of 8.6±3.5 cm s^{-1}. Note that the station pair north of the SAF (31-32) also shows a strong eastward bottom velocity; this estimate should be viewed with caution, however, because the SADCP depth range was only 200 m (Figure 3). Two station pairs south of 54°S show westward bottom velocities that exceed the SADCP reference error. These velocity profiles (not shown) are monotonic, eastward in the upper ocean and going through zero near 2000 m depth; they are among the few profiles for which a good "level of no motion" can be found.

4.4. P17 135°W

P17 lies above the East Pacific Rise and has the minimum deepest common level for the SAF station pairs ($\sim$2500 m) among the six lines. Surface flow is mainly southeast with a small intense cyclone at 54.5°S (Plate 3). The SADCP reference shows three regions of eastward bottom flow near 4 cm s^{-1} separated by three station pairs with zero or westward bottom velocities. Here we have the largest curvature correction for the small intense cyclone adjacent to the SAF: The inferred bottom velocity for the station pair 76-77 changes from 4.2 cm s^{-1} westward to 3.6 cm s^{-1} eastward. This station pair is within the SAF. P17 also has the weakest eastward SAF bottom velocities (3.6±3.0 cm s^{-1}).

4.5. P17E 126°W

The SADCP reference is applied only to the SAF station pair and the four station pairs to the south of the SAF due to failure of the GPS heading measurement (Plate 3). Within the SAF the eastward bottom velocity is 11.9±2.5 cm s^{-1} at the northern SAF station pair. South of the SAF the SADCP reference is not different from referencing to the bottom.

4.6. P19 88°W

Along P19 the surface velocity vectors are mainly eastward except for the cyclonic eddy centered near
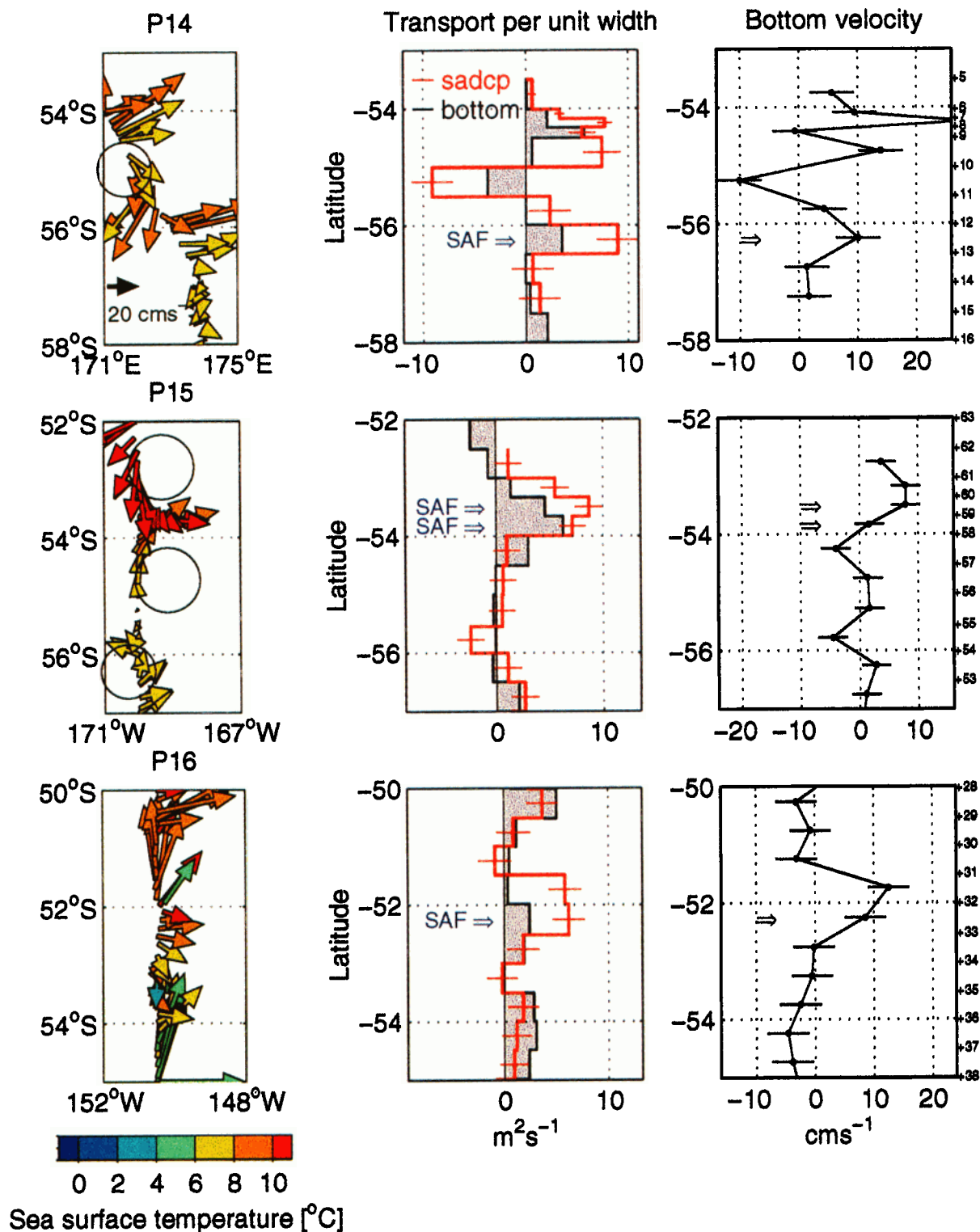
Plate 2. SADCP velocities, transports, and bottom velocities are shown for (top) P14, (middle) P15, and (bottom) P16. SADCP velocity vectors (averaged over 150-250 m and color coded by sea surface temperature) in the left panels distinguish the SAF jets from adjacent eddies (shown schematically by black circles). Between-station transports per unit width determined by referencing the geostrophic shears to zero at the deepest common level (black) and to the SADCP (red) are shown in the middle panels. In the right panels, bottom velocities determined from the SADCP reference show that strong bottom (>3 cm s^{-1}) velocities can be found in the eddies and that bottom velocities are eastward within the SAF. Error bands for the SADCP-referenced bottom velocity (Table 2) and transport are plus or minus one standard deviation. Positive transports and velocities are eastward. Bottom velocity estimates are omitted on parts of P14 and P15 because of SADCP data dropouts.
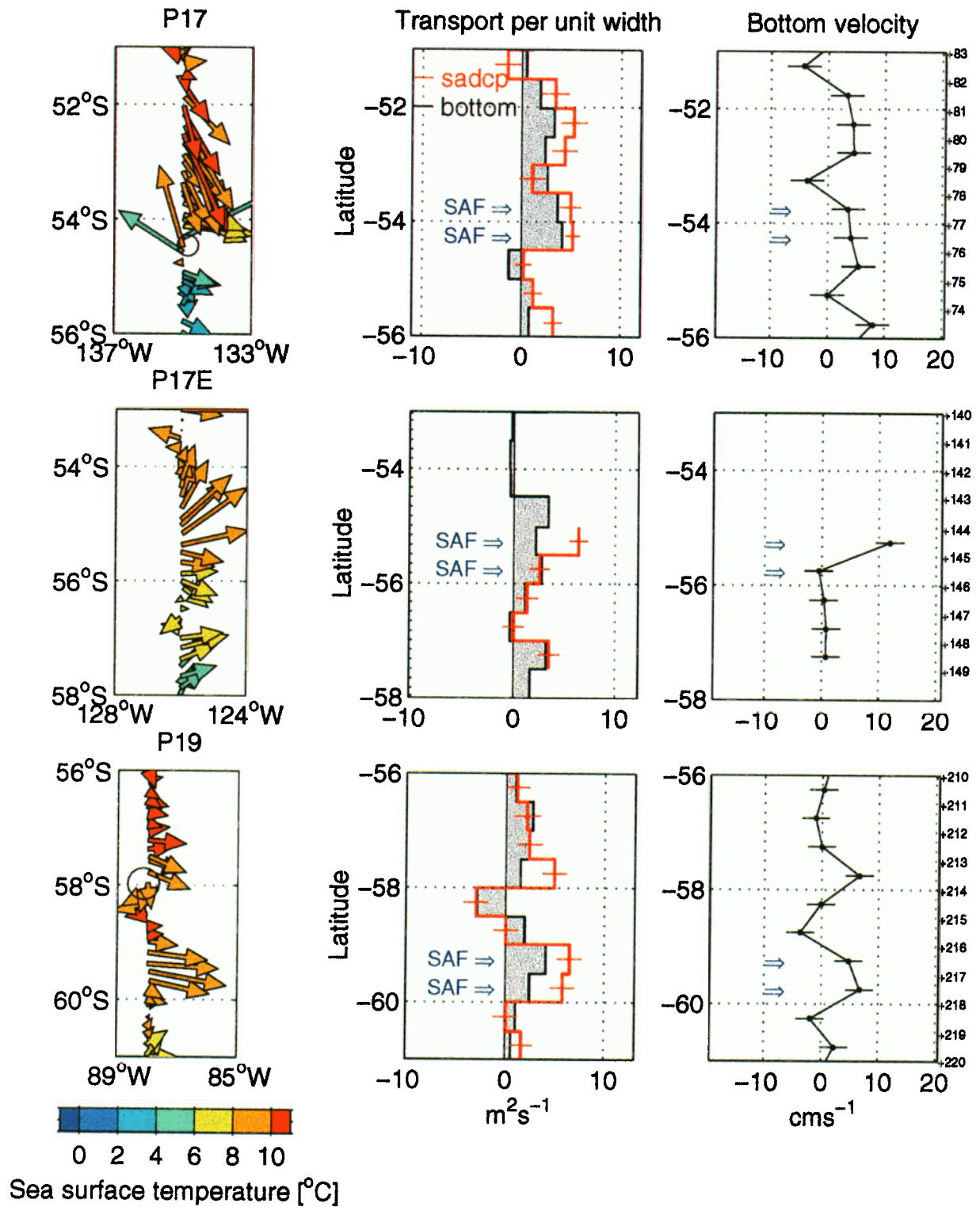
Plate 3. Same as Plate 2 but for (top) P17, (middle) P17E, and (bottom) P19. Bottom velocity estimates are omitted on parts of P17E because of a failure of the GPS heading measurement.
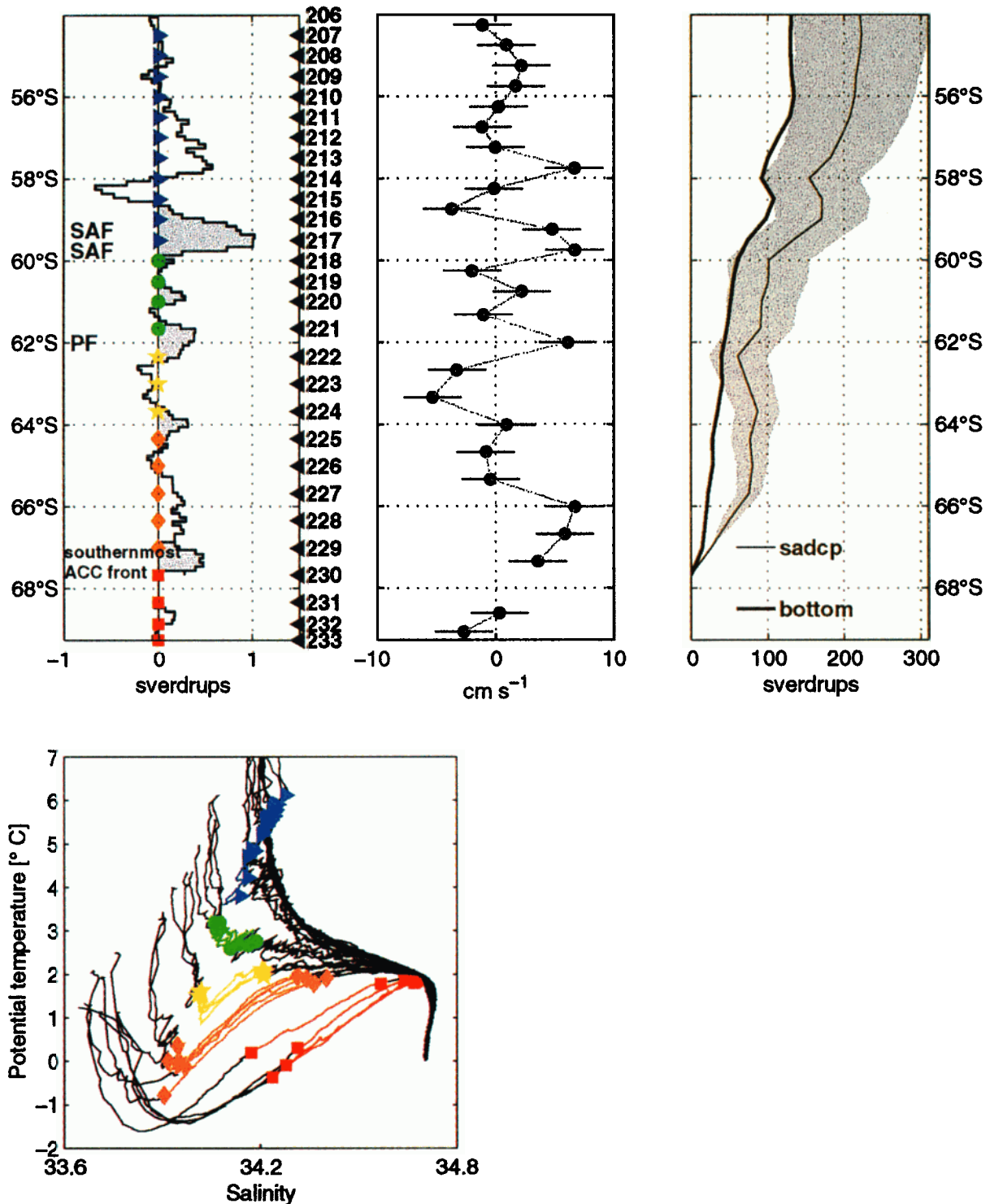
Plate 4. SADCP cross-track transport (left panel) between 150 and 350 m along P19 88°W reveals five narrow jets (shaded gray) which contribute 73% of the total eastward upper ocean transport across the section. Stations with similar potential temperature-salinity (θ-S) properties (bottom panel) are grouped and assigned a color and symbol. For each station, θ-S values between 150 and 350 m are plotted with color-coded lines, and color-coded symbols are plotted for the 150 and 350 m values. These colored symbols are also plotted on the SADCP transport plot (left panel).The region north of the SAF is all one color because there is not such a clear grouping of θ-S profiles as further south. The four voids in θ-S space, indicative of water mass changes, coincide with four surface jets. Bottom velocity determined from the SADCP reference (middle panel) shows eastward (positive) velocities beneath the five jets. Geostrophic stream function is shown in the right panel (thin, SADCP; thick, bottom reference). The SADCP transport error (gray shading) quickly accumulates along the section. The Polar Front (PF) and southernmost Antarctic Circumpolar Current (ACC) front are identified using the definitions of *Orsi et al.* [1995].
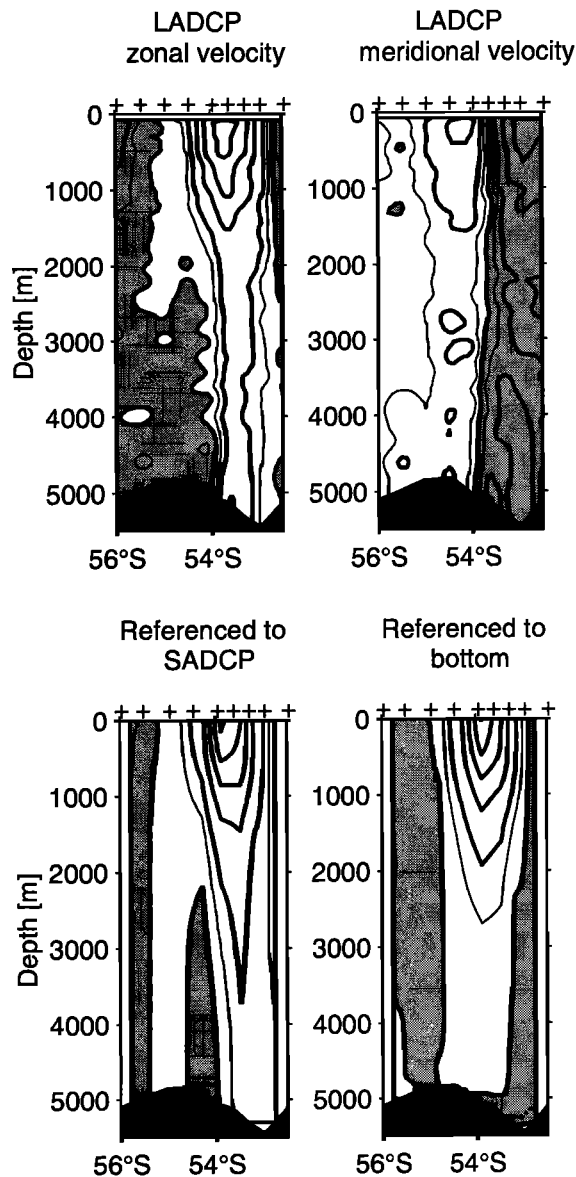
Figure 4. The LADCP zonal velocities from P15, 170°W (upper left) show that the eastward flow associated with the SAF extends throughout the water column. The LADCP zonal velocity better resembles the SADCP-referenced geostrophic velocity (lower left) than the bottom-referenced estimate (lower right). The LADCP meridional velocities (upper right) also show the deep penetration of the surface flows, and reveal strong meridional convergence into the SAF throughout the water column. Westward and southward velocities are shaded. The main contour interval is 10 cm s⁻¹, with thin contours at ±5 cm s⁻¹.

58°S (Plate 3). Transports referenced to the bottom are similar in direction to the surface cross-track velocity. SADCP-referenced bottom velocities are eastward for the SAF station pairs (4.8 ± 2.4 cm s⁻¹ and 6.7 ± 2.4 cm s⁻¹). Additional eastward bottom velocity of 6.7 ± 2.4 cm s⁻¹ is found within the northern part of the cyclone (station pair 213, 214). The curvature adjustment decreases the bottom velocity at this station

pair by 1.2 cm s⁻¹. The bottom velocity for the station pair north of the SAF is westward; the velocity profile shows a transition from eastward flow to westward flow at 2500 m.

5. Transports Within the SAF

Zonal transports near the SAF may be calculated using any of several referencing schemes (Table 4). The choice of lateral boundaries is subjective and arbitrary; the purpose of the calculation is to illustrate the sensitivity of transport to the choice of reference level for a given section. Here we include the SAF station pairs and extend the northern and southern limits to the nearest reversal in transport or the nearest minimum in eastward transport. For P17E the northern boundary of the SAF geostrophic jet is the northernmost SADCP-referenced station pair. We assume that the SADCP instrument error acts as a bias, while the semidiurnal internal tide and near-inertial errors are uncorrelated from one station pair to the next. Transport error is given as one standard deviation. Transports are calculated relative to and above three reference levels (2500 m, 3000 m, and the bottom).

Among zero-reference schemes, the bottom reference yields the largest transport. The difference can be substantial. For example, P15 and P19 transports relative to the bottom are about 20 Sv larger than those referenced to 2500 m, reflecting the tendency for geostrophic shear to maintain its sign while decreasing in magnitude below 2500 m, as shown in Figure 1. As expected, the SADCP-referenced transports are much larger than any of the reference level estimates due to the eastward bottom velocities within the SAF station pairs. SADCP-referenced transports are 1.1 to 2.6 times as large as the bottom-referenced transports. Five of the six lines (P14, P15, P16, P17E, and P19) have SADCP-referenced transports that differ from the bottom reference by more than one standard deviation.

6. SADCP-Referenced ACC on P19

The SADCP resolves the horizontal scales of the narrow fronts and current cores characteristic of the ACC. The SADCP cross-track transport (Plate 4, top left panel) is concentrated in five narrow jets which contribute 60% of the total eastward upper ocean transport. Four voids in potential temperature-salinity space, showing water mass fronts, coincide with surface jets (Plate 4, bottom panel). Several of the current cores are only 50–100 km wide; the horizontal structure of the currents is not well resolved by the standard 55-km WHP hydrographic station spacing. Transports may be seriously overestimated or underestimated if based on currents measured on-station only (e.g., LADCP), or if only on-station SADCP measurements were used as a geostrophic reference. Integration of the underway data between stations is crucial.

Table 4. Eastward Geostrophic Transports Within the SAF for Each Line as a Function of Geostrophic Reference Technique[a]

Line	Latitudinal Range	Eastward Geostrophic Transport, Sv			
		2500 m	3000 m	Bottom	SADCP
P14	56.49°S to 55.99°S (13 to 12)	17	18	23	57 ± 13[b]
P15	54.50°S to 53.00°S (57 to 61)	42	48	61	83 ± 13[b]
P16	53.00°S to 51.99°S (34 to 32)	19	22	25	46 ± 13[b]
P17	54.49°S to 53.01°S (76 to 79)	52	56	58	62 ± 11
P17E	56.51°S to 55.02°S (147 to 144)	25	27	34	56 ± 11[b]
P19	61.00°S to 58.50°S (220 to 215)	33	39	56	78 ± 20[b]

[a]Lateral boundaries are subjective and arbitrary; the value of the calculation is to illustrate the sensitivity of transport to the choice of reference level. Station ranges are given in parenthesis.

[b]SADCP transports exceed the bottom reference transports by more than one standard deviation.

Except between stations 230 and 231, the SADCP data quality along P19 is adequate for geostrophic referencing. ACC geostrophic cross-track bottom velocities tend to be in the direction of the geostrophic surface velocities over most of the region (Plate 4, top middle panel). As in the SAF, eastward bottom velocities are present beneath the two other major ACC fronts, the Polar Front (PF) and the southern ACC front [*Orsi et al.*, 1995]; their respective magnitudes are 6.1±2.4 and 3.6±2.4 cm s⁻¹.

SADCP-referenced ACC transport and error estimates illustrate the need for velocity accuracy that is probably beyond any foreseeable SADCP capability (Plate 4, top right panel). Integrated from 66.7°S to 54°S, the transport uncertainty accumulates to 90 Sv, primarily owing to the 1 cm s⁻¹ SADCP bias estimate. The SADCP-referenced transport of 221±90 Sv differs from the bottom-referenced transport (131 Sv) by only one estimated standard deviation.

7. ACC Sections in the POP Model

Numerical models do not have the same sort of limit on transport accuracy as SADCP-referenced geostrophic calculations do, so we show here a preliminary look at the ACC in POP. We consider four sections: 170°E, 170°W, 150°W, and 88°W, which correspond to the WHP lines P14, P15, P16, and P19 (Plates 2 and 3 and Figure 4), and which illustrate differing positions of the SAF relative to topography (Plate 1). To avoid dealing explicitly with temporal variability, we show only the 1992 annual average (Figure 5). In spite of the temporal averaging, the pattern of currents looks similar to observations; there is the same tendency for the zonal component of near-bottom velocity to take the same sign as the surface velocity. Near-bottom velocity zonal components locally exceed 5 cm s⁻¹ in magnitude.

To simulate a bottom-referenced geostrophic section, the velocity from the deepest grid point was subtracted from each POP velocity profile. The difference in the transport stream function between these bottom-refer-

enced velocities and the actual velocity differs from section to section and as a function of latitude on each section (Figure 5, bottom panels). The 170°E section is bounded by Antarctica on the south and the Campbell Plateau on the north. The total transport exceeds the bottom-referenced transport by 28 Sv. At the southern end of the section, the bottom reference indicates a large eastward transport where in fact the transport is westward. At 170°W and 150°W the net transport between Antarctica and 45°S is close to the bottom-referenced estimate, but the latter misses a recirculation of over 40 Sv south of the Southeast Pacific Rise in each section. On 88°W the bottom-referenced stream function at 45°S exceeds the true stream function by 37 Sv, with major contributions coming from the continental slope of Antarctica and at the north end of the section. Hence in POP, at least, a bottom reference can overestimate or underestimate the transport.

8. Discussion and Conclusions

Two questions were posed in section 1: Does the bottom reference distort the horizontal velocity structure? If so, does it bias estimates of the ACC transport? The SADCP-referenced WHP sections provide a clear affirmative answer to the first question and a partial answer to the second; at least locally in the SAF, the transport is biased low. Our cursory look at output from the POP model suggests that the dominant tendency of bottom referencing is to bias the entire ACC transport estimate low, but that the amount of bias varies from region to region.

The zonal component of near-bottom velocity tends to coincide in direction with the surface geostrophic velocity, so at all depths, bottom-referenced geostrophic currents tend to underestimate the actual cross-track currents, averaged between stations. In addition, hydrographic station spacing rarely resolves the narrow jets in the ACC well, so regardless of referencing method, geostrophic current calculations give a distorted picture of the number, width, and speed of the jets and eddies
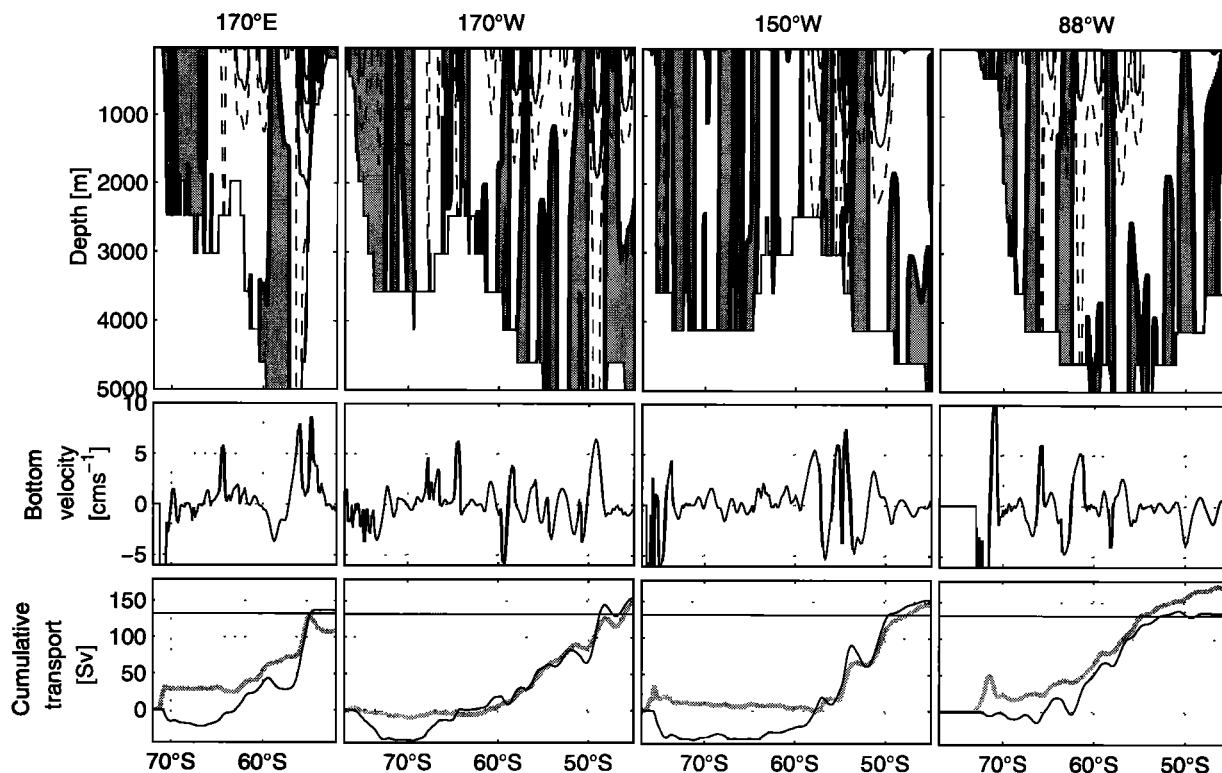
Figure 5. (top) Contours of zonal velocity for four longitudinal slices of the POP11 1992 annual mean, showing that eastward flow in the ACC jets extends to the bottom. The main contour interval is 10 cm s^{-1}, with dashed contours at ±5 cm s^{-1}. Westward velocities are shaded. (middle) Zonal component of bottom velocity. (bottom) Transport stream function from the full velocity field (thin line) and from the velocity minus the bottom velocity (thick shaded line). The thin horizontal line at 132 Sv shows the model transport through Drake Passage averaged over 1992.

in the ACC. In the SAF a bottom reference systematically underestimates the eastward flow (Tables 3 and 4), sometimes by a factor of 2 or more. Bottom velocities range from 4 to 10 cm s^{-1}, and can change by as much as 12 cm s^{-1} over 50 km. Recent analysis by H. E. Phillips and S. R. Rintoul (A mean synoptic view of the Subantarctic Front south of Australia, submitted to *Journal of Physical Oceanography*, 2000) of a current meter array within the SAF along 143°E (WHP line SR3) is consistent with our result. They estimate that a bottom reference underestimates the eastward SAF transport by 14%.

Although the SADCP can provide a much better picture of the horizontal structure of currents in the ACC region than can geostrophic calculations, SADCP referencing can not provide accurate transport estimates for the entire ACC. First, ACC sections usually include regions of poor SADCP quality due to bad weather, and regions of large ageostrophic velocities. Second, full-depth transport estimation is extremely demanding of velocity accuracy; a bias of only 1 cm s^{-1} in a 4600-m deep ocean causes a 5-Sv transport error per degree of latitude.

Instead of directly referencing single sections, SADCP velocities can be used in an inverse model. For exam-

ple, a recent Southern Ocean calculation [*Gille*, 1999] included two types of velocity measurements as constraints: SADCP upper ocean velocities and 1000-m drift vectors from Autonomous Lagrangian Circulation Explorers (ALACE). The solution was insensitive to the velocity measurements; it seems they were inconsistent with the physics of the inverse model. Several factors may be responsible. First, in places the SADCP velocity includes a large ageostrophic component. Second, the spatial and temporal sampling by ALACE floats may be a poor match for the hydrographic sections. Third, the SADCP velocities, and presumably the ALACE drifts, are inconsistent with the model's initial state of zero bottom flow. If multiple solutions exist, the inverse model will favor the solution closest to the initial condition. Fourth, SADCP velocities were available only for a few of the boundaries.

An accurate representation of the reference level velocities may not be necessary to determine property fluxes through the boundaries of an inverse model. *McIntosh and Rintoul* [1997] explored the performance of several inverse models using FRAM output. They found that when interfacial fluxes are included as unknowns and column weights are chosen correctly, the property fluxes are accurate even though the result-

ing reference level velocities are smoothly varying and poorly represent the actual FRAM velocities. *McIntosh and Rintoul* [1997, p. 306] stated, "The successful flux estimates reflect the fact that the variability of the reference level velocity on small spatial scales does not carry a significant net flux of heat or salt."

Unlike the net property fluxes, the fundamental dynamical balances of the ACC cannot be determined without an accurate representation of the velocity field. In particular, the eastward flow that we find in the SAF beneath the Drake Passage sill depth must recirculate on local and/or gyre scales. The nature of these deep recirculations warrants further investigation. The dynamical role of bottom topography also depends critically on the bottom velocities.

The Parallel Ocean Program (POP) high-resolution global ocean model, which produces a realistic ACC transport at Drake Passage [*Maltrud et al.*, 1998], shows deep-reaching eastward velocities within the ACC jets similar to observations. A preliminary look at the 1992 transport stream function on four sections shows that the effect of bottom referencing varies from section to section; it can cause 40-Sv recirculations to be missed and can cause net transport to be underestimated or overestimated by O (30 Sv). We believe that more extensive analyses of output from POP and other high-resolution models will be highly rewarding in future studies of ACC transport and dynamics.

Appendix A: Error Estimation for Geostrophic Referencing

The largest errors in the ADCP reference velocity estimates usually come from internal tides and near-inertial oscillations. We have developed a crude method to estimate the magnitude of these errors from the ADCP data set itself. The key assumptions are (1) that the dominant causes of velocity change during each station are indeed semidiurnal internal tides and near-inertial oscillations, and (2) that the former has a larger vertical scale of variability than the latter.

A.1. Estimating Internal Tide and Near-Inertial Oscillation Amplitudes from on-Station Velocity Measurements

To separate these components from each other and from the remainder of the internal wave spectrum, the on-station SADCP velocity time series, $u(z, t)$, is first separated by least squares fitting into two parts:

$$u(z, t) = u_p(z, t) + u_r(z, t), \qquad (2)$$

where

$$u_p(z, t) = \sum_{m=1}^{2} \sum_{n=1}^{2} a_{mn} z^m t^n \qquad (3)$$

is slowly varying in z and t, and u_r, the residual, varies rapidly in z and/or t. We assume the temporal variability of u_p is mostly caused by the semidiurnal tide. The

tidal amplitude A_{sd} is then estimated from the vertical mean (denoted by an overbar) of u_p by the following least squares fit:

$$\overline{u_p(t)} = A_{sd} \exp(-i\omega t + \phi) + \text{residual}, \qquad (4)$$

where ω is the frequency of the M_2 semidiurnal constituent, and ϕ is a phase. (For convenience of notation, the velocity vector is represented as a complex number: $u = u + iv$.) That is, we assume the semidiurnal tidal current is rotating anticyclonically, and we are fitting the fraction of a cycle that occurs during a station. With such a small fraction of a cycle, we make no attempt to distinguish between a current ellipse and a circle.

The amplitude of the near-inertial energy was estimated as the time and depth average of $|u_r|$. Near-inertial energy is prominent in $u_r(z, t)$. At each depth, u_r tends to rotate anticyclonically with time, and when this rotation rate is averaged over depth and over groups of stations, it typically approximates the local inertial frequency (not shown).

A.2. Effect of Internal Tides and Near-Inertial Oscillations on the SADCP Reference Estimate

The expected error in ADCP reference velocity from the internal tide is smaller than the tidal amplitude. Although it is possible for the ship's velocity to Doppler shift the internal tide to zero frequency, so that the entire tidal amplitude appears as an ageostrophic velocity between a pair of stations, this will be a rare event. Equally rare will be the situation in which an integral number of cycles is sampled between a station pair, so that the error is zero. For our error estimates here, we suppose that the space-time averaging of the tide between stations reduces the velocity variance by 50%, averaged over an ensemble of stations along cruise tracks in various locations.

Near-inertial oscillations have large horizontal scales, so the horizontal averaging between stations is ineffective in reducing the variance, and the time between stations also causes only a small reduction. If the vertical scale of the near-inertial motions is small compared to the vertical averaging interval of the reference layer, then there will be a negligible contribution to the reference velocity. To be conservative, however, we treat the mean amplitude of u_r as an index of the near-inertial motion and higher-frequency internal waves that might be present throughout the reference layer, and we simply add the square of this index to the other sources of reference layer variance.

Many objections may be raised to this error estimation scheme, and undoubtedly it can be improved; but we believe it has value for the present study nevertheless. A fundamental objection is that the method estimates the amplitudes of two periodic constituents using time series much shorter than either period; each on-station time series is typically 2–4 hours. The esti-

mates are therefore noisy at best. To reduce the noise, estimates are regionally averaged along a section. Evidence that a signal emerges includes a tendency for larger internal tide estimates to coincide with rougher topography (in the present data set and in others we have studied) and for the rotation rate of u_r to match the local inertial frequency. Furthermore, the estimates are conservative. The low vertical wave number part of the near-inertial field contributes to u_p, biasing the estimated tidal contribution high, and as noted above, the vertical average of the amplitude of u_r is certainly an overestimate of the contribution of u_r to the reference velocity.

References

Cokelet, E. D., M. L. Schall, and D. M. Dougherty, ADCP-referenced geostrophic circulation in the Bering Sea Basin, *J. Phys. Oceanogr.*, *26*, 1113–1128, 1996.

Daly, K. L., W. O. Smith, G. C. Johnson, G. R. DiTullio, D. R. Jones, C. W. Mordy, R. A. Feely, D. A. Hansell, and J. Z. Zhang, Hydrographic structure and distributions of nutrients and particulate and dissolved carbon in the Pacific sector of the Southern Ocean, *J. Geophys. Res.*, *106*, 7107–7124, 2001.

Egbert, G. D., A. F. Bennet, and M. G. Foreman, TOPEX/POSEIDON tides estimated using a global inverse model, *J. Geophys. Res.*, *99*, 24,821–24,852, 1994.

Fischer, J., and M. Visbeck, Deep velocity profiling with self-contained ADCP's, *J. Atmos. Oceanic Technol.*, *10*, 764–773, 1993.

Gille, S. T., Mass, heat, and salt transport in the southeastern Pacific: A Circumpolar Current inverse model, *J. Geophys. Res.*, *104*, 5191–5209, 1999.

Grose, T. J., J. A. Johnson, and G. R. Bigg, A comparison between the FRAM (Fine Resolution Antarctic Model) results and observations in the Drake Passage, *Deep Sea Res.*, *42*, 365–388, 1995.

Hacker, P., E. Firing, D. Wilson, and R. Molinari, Direct observations of the current structure east of the Bahamas, *Geophys. Res. Lett.*, *23*, 1127–1130, 1996.

Heywood, K., M. Sparrow, J. Brown, and R. Dickson, Frontal structure and Antarctic Bottom Water Flow through the Princess Elizabeth Trough, Antarctica, *Deep Sea Res.*, *46*, 1181–1200, 1999.

Holton, J. R., *An Introduction to Dynamic Meteorology*, Academic, San Diego, Calif., 1979.

Joyce, T., On in situ calibration of shipboard ADCPs, *J. Atmos. Oceanic Technol.*, *6*, 169–172, 1989.

Killworth, P. D., An equivalent-barotropic mode in FRAM, *J. Phys. Oceanogr.*, *22*, 1379–1387, 1992.

King, B. A., and E. B. Cooper, Comparison of ship's heading determined from an array of GPS antennas with heading from conventional gyrocompass measurements, *Deep Sea Res.*, *40*, 2207–2216, 1993.

Maltrud, M. E., R. Smith, A. Semtner, and R. Malone, Global eddy-resolving ocean simulations driven by 1985-

1995 atmospheric winds, *J. Geophys. Res.*, *103*, 30,825–30,854, 1998.

McCartney, M. S., Subantarctic mode water, in *A Voyage of Discovery, George Deacon 70th Anniversary Volume*, edited by M. Angel, pp. 103–119, Pergamon, Tarrytown, N.Y., 1977.

McCartney, M. S., The subtropical recirculation of mode waters, *J. Mar. Res.*, *40*, 427–464, 1982.

McIntosh, P., and S. R. Rintoul, Do box inverse models work?, *J. Phys. Oceanogr.*, *27*, 291–308, 1997.

McTaggart, K. E., and G. Johnson, CTD/O2 measurements collected on a Climate and Global Change cruise (WOCE Sections P14S and P15S) during January-March, 1996, *Tech. Rep. ERL PMEL-63* (available as *PB98-110158* from Natl. Tech. Inf. Serv., Springfield, Va.), Pac. Mar. Environ. Lab., NOAA, Seattle, Wash., 1997.

McTaggart, K. E., G. Johnson, and B. A. Taft, CTD/O2 measurements collected on a Climate and Global Change Cruise (WOCE Section P18) along 110°W during January-April, *Tech. Rep. ERL PMEL-59*, Pac. Mar. Environ. Lab., NOAA, Seattle, Wash., 1996.

Meinen, C. S., D. R. Watts, and R. A. Clarke, Absolutely referenced geostrophic velocity and transport on a section across the North Atlantic Current, *Deep Sea Res.*, *47*, 309–322, 2000.

Nowlin, W. D., and M. Clifford, The kinematic and thermohaline zonation of the Antarctic Circumpolar Current at Drake Passage, *J. Mar. Res.*, *40*, 481–505, 1982.

Orsi, A. H., T. Whitworth, and W. D. Nowlin, On the meridional extent and fronts of the Antarctic Circumpolar Current, *Deep Sea Research*, *42*, 641–673, 1995.

Pickart, R. S., and S. S. Lindstrom, A comparison of techniques for referencing geostrophic velocities, *J. Atmos. Oceanic Technol.*, *11*, 814–824, 1994.

Pollard, R., and J. Read, A method for calibrating ship-mounted acoustic Doppler profilers and the limitations of gyro compasses, *J. Atmos. Oceanic Technol.*, *6*, 859–865, 1989.

Read, J. F., R. T. Pollard, I. I. Morrison, and C. Symon, On the southerly extent of the Antarctic Circumpolar Current in the southeast Pacific, *Deep Sea Res.*, *42*, 933–954, 1995.

Rubin, S., J. Goddard, D. Chipman, T. Takahashi, S. Sutherland, J. L. Reid, J. Swift, and L. Talley, Carbon dioxide, hydrographic, and chemical data obtained in the South Pacific Ocean (WOCE Section P16A/P17A, P17E/P19S, and P19C, R/V "Knorr", October 1992-April 1993 , *Tech. Rep. ORNL/CDIAC-109*, Oak Ridge Natl. Lab., Oak Ridge, Tenn., 1998.

Saunders, P. M., and B. A. King, Bottom currents derived from a shipborne ADCP on WOCE cruise A11 in the South Atlantic, *J. Phys. Oceanogr.*, *25*, 329–347, 1995.

Webb, D., P. D. Killworth, A. Coward, and S.R.Thompson, *The FRAM atlas of the Southern Ocean*, Natural Environment research Council, Swindon, U.K., 66 pp., 1991.

Whitworth, T., and W. D. Nowlin, Water masses and currents of the Southern Ocean at the Greenwich Meridian, *J. Geophys. Res.*, *92*, 6462–6476, 1987.

Whitworth, T., W. D. Nowlin, and S. J. Worley, The net transport of the Antarctic Circumpolar Current through Drake Passage, *J. Phys. Oceanogr.*, *12*, 960–971, 1982.

S. Chen, E. Firing Oceanography Department, 1000 Pope Road, Honolulu, HI 98622. (schen@soest.hawaii.edu;efiring@soest.hawaii.edu)

K. A. Donohue Graduate School of Oceanography, 215 South Ferry Road, Narragansett RI 02882. (kdonohue@gso.uri.edu)